Journal of Orthopaedic Translation (2015) 3, 105—113

Available online at www.sciencedirect.com

ScienceDirect

journal homepage: http://ees.elsevier.com/jot

ORIGINAL ARTICLE

Novel nanocomposite biomaterial to differentiate bone marrow mesenchymal stem cells to the osteogenic lineage for bone restoration

Arun Kumar [a,*], Chelsea Young [b], Juliana Farina [c], Ashley Witzl [c], Edward D. Marks [a]

[a] *Nanomedicine Research Laboratory, Department of Medical Laboratory Sciences, College of Health Sciences, University of Delaware, Newark, DE, USA*
[b] *Department of Chemical Engineering, College of Engineering, University of Delaware, Newark, DE, USA*
[c] *Department of Biological Sciences, College of Health Sciences, University of Delaware, Newark, DE, USA*

Received 9 November 2014; received in revised form 22 February 2015; accepted 10 March 2015
Available online 28 April 2015

KEYWORDS
chitosan;
crosslinking;
mineralization;
nanocomposite;
three-point analysis

Summary *Background/Objective:* As the bone engineering field moves away from nonviable implants to more biocompatible and natural structures, nanomedicine has emerged as a superior tool for developing implantable materials.
Methods: Here, we describe the fabrication and testing of a nanocomposite structure composed of chitosan and a biocompatible thermoplastic (PMMA).
Results: Our nanocomposite material displayed morphologically similar characteristics to an extracted murine femur during microscopic and spectroscopic analysis as seen through SEM and FTIR. Crosslinking our nanocomposite enhanced structural and strength characteristics significantly above the noncrosslinked sample, mimicking the strength of an extracted mammalian bone. When cocultured with bone marrow mesenchymal stem cells, the composite material proved to be osteoinductive and osteogenic via DAPI and actin staining, differentiating BMSCs into the osteogenic lineage and promoting mineral deposition. Nodule formation, indicative of mineralization during BMSC differentiation, was confirmed spectroscopically via FTIR and autofluorescence of the nodule.

* Corresponding author. Nanomedicine Research Laboratory, Department of Medical Laboratory Sciences, College of Health Sciences, 305C Willard Hall, University of Delaware, 16 West Main Street, Newark, DE 19716, USA.
E-mail address: arunk@udel.edu (A. Kumar).

http://dx.doi.org/10.1016/j.jot.2015.03.002

Conclusion: These encouraging results show promise for *in vivo* implantation of our novel scaffold that is both biocompatible and biomimetic in strength and composition.

Introduction

Transplantable grafts are two major types: the autograft and the allograft. Autograft transplantations occur when tissues are transferred directly from an unaffected portion of the patient's body to the wounded area. Because the tissue is from the same body, rejection risk is significantly decreased. However, other risks, such as donor-site morbidity, bone availability, and unpredicted graft resorption, have been associated with this procedure [1]. Allografts use tissue from an outside source, commonly a bone bank. Because the tissue is not the patient's own tissue, there are higher risks of rejection. The patient's immune system may recognize the transplant as an antigen and trigger a protective response [2].

Recently, synthetic bone materials have been developed to overcome many of the obstacles listed above [3–5]. To integrate better with the body, a synthetic bone material must be biocompatible and accurately mimic the physical structure of natural bone [6]. Osteoinductive and osteogenic potential of the material is also crucial to ensure differentiation and proliferation of *in vivo* cellular networks [7,8]. Chitosan, a polysaccharide obtained by the alkaline deacetylation of chitin [9], has a number of characteristics that make it an adequate substance to use as a bone replacement polymer platform, including its biodegradability [10], biocompatibility [11], and nontoxic nature [12]. The structural instability of chitosan warrants strengthening when used in chronic loading conditions (such as femur bone synthesis) [13], so the addition of other polymers can aid in mechanical strength [14,15].

As others have found before [16,17], the structural instability of chitosan warrants the addition of a strengthening element, usually through the process of crosslinking. Polymers, such as polyvinyl alcohol and polymethylmethacrylate (PMMA), both types of biocompatible plastic [18], are often added to aid in structural stability. Chitosan/polymer mixes for the development of skin and organ scaffolds do not need this increased stability, but the literature has shown [19] that without tertiary additions a composite cannot hope to exceed the strength of a dental cavity, let alone a femur. Our strength studies show that an addition of 2% of 2-hydroxyethyl starch significantly aided structural stability.

Herein, we describe the successful development of a novel nanocomposite bone material derived from crosslinked chitosan. We demonstrate the nanocomposite's favourable comparison to an extracted femur, both in strength and morphology. Further, we establish the biocompatibility of the nanocomposite by coculturing the material in proximity of bone marrow-derived mesenchymal stem cells (BMSCs), which appear to begin osteogenic differentiation compared to cells outside the nanocomposite's proximity.

Materials and methods

Murine bone preparation

Animal samples were obtained from experiments that were conducted ethically in accordance with the University of Delaware's Institutional Animal Care and Use Committee guidelines for the use and care of animals (University of Delaware, Newark, DE, USA). Mice sacrificed with CO_2 had one hind femur extracted and as much excess tissue as possible was physically removed. The bones were more thoroughly cleaned using a three-step wash. Briefly, bones were soaked in chloroform for 1 minute to soften the tissue for easier physical removal. The bone was then rinsed with distilled water. The procedure was repeated two more times using acetone then ethanol as the solvent. Cleaned bones were stored at 4°C.

Polymerization and preparation of nanocomposite bone material

Chitosan (MW 100,000–300,000) was purchased from Acros Organics (Morris Plains, NJ, USA). Chitosan need was calculated with the following equation:

$$\frac{x}{y+x}=\frac{z}{100} \quad (1)$$

where x represents solid chitosan weight, y solvent volume, z percentage w/v of the final solution. Once measured, chitosan was dissolved in two beakers with a 2% acetic acid stock solution. When the chitosan was fully dissolved, the ground nanocomposite bone material was added to each beaker and homogenized. The resulting substance was left to dry on an Isotemp hotplate (Fisher Scientific, Waltham, MA, USA) set at 55°C.

Two percent w/v PMMA (Acros Organics) was added to the sample for structural stability. An appropriate amount PMMA was dissolved in chloroform. The dried chitosan sample was ground up and added to the beaker with the dissolved PMMA. Two percent w/v 2-hydroxyethyl starch (Spectrum Chemical, Gardena, CA, USA) was added using the same process as PMMA, except warm water was used as a solvent rather than chloroform. The resulting substance was left to dry overnight.

A rectangular prism shape was formed from the sample in order to allow for physical experimentation. When the

final sample was almost dry, but still pliable, it was removed from the beaker and placed onto a sheet of foil, where it was manually shaped into a rectangular prism of approximate size 10 mm × 3 mm × 4 mm. It was then allowed to dry on a hotplate set to 60°C.

Fourier transformed infrared spectroscopy

A Nicolet iS5 spectrometer with an iD5 ATR diamond tip adapter (Thermo Scientific, Waltham, MA, USA) was used to perform Fourier transformed infrared spectroscopy (FTIR). The samples were ground and dissolved in their respective solvents, and 10 μL was placed at the diamond tip/sample interface. Samples were measured to determine characteristic peaks relating to bond stretching and rocking, using the respective solvents as a blank. The FTIR analysis was carried out over a wave number range between 4000 cm^{-1} and 400 cm^{-1} at a resolution of 2 cm^{-1}.

Scanning electron microscopy analysis

Scanning electron microscopy (SEM) was performed to visualize the mammal bone sample and two 6% chitosan samples. The four samples were sliced with a microtome and mounted on aluminium mount-M4 sample holders (Electron Microscopy Sciences, Hatfield, PA, USA) and placed in a Denton Bench Top Turbo III vacuum chamber (Denton Vacuum, Moorestown, NJ, USA) for coating with a 50:50 mix Au:Pd to aid visualization. The samples were placed into the microscope (S4700; Hitachi High Technologies, Tokyo, Japan) and images were taken from 1800× to 15,000× magnification.

Three-point analysis

Three-point analysis was performed on an RSA G2 solids analyser (Texas Instruments, Dallas, TX, USA). Samples measuring 10 mm × 3 mm × 4 mm were placed on two bottom pressure points that doubled as support structures. A computer recorded a third shaft's force applied to the sample at 0.4 N/s and displacement Z-height of said shaft calculated as distance from Point 0 (top of the sample) moving at approximately −8.75 μm/s.

Cell culture

A composite bone material of approximate dimensions 3 mm × 4 mm × 3 mm was placed in a 10 cm^2 petri dish. To sterilize, the composite material was left in the open dish in the culture hood under UV light for 1 hour. BMSCs (StemCell Technologies, Vancouver, BC, Canada) were plated around the composite material at a density of 3×10^5 cells/mL, and 3–4 mL of noncomplete MesenCult basal media (StemCell Technologies) was added. Cells were incubated at 37°C and 5% CO_2 for 3 days in a Forma Steri-Cycle CO_2 Incubator (Thermo Scientific) with images taken every 24 hours. At the end of 72 hours, the media and composite material were removed from the culture. Cells were fixed in 4% paraformaldehyde in phosphate buffered saline (PBS) for 10 minutes and washed three times for 3 minutes each in PBS. ActinRed 555 and NucBlue Molecular Probes stains (Life Technologies, Carlsbad, CA, USA) were prepared in PBS as per company specifications and incubated on cells for 20 minutes. Cultures were then washed in PBS three times for 3 minutes and imaged using an Evos FL fluorescence microscope (Thermo Scientific).

Statistical analysis

The statistical significance of the results was determined using analysis of variance (ANOVA) and a multiple means comparison function (*t* test) in JMP (SAS Institute Inc., Cary, NC, USA) with an α level of 0.05. All error bars are reported in mean ± standard error from the mean, with $n = 3$ unless otherwise noted.

Results

Sample construction

Concentrations of chitosan samples of 2%, 4%, 6%, and 8% w/v were developed and assessed for structural stability. The 2% and 4% samples crumbled immediately upon contact with the instruments, and purity and ease of use issues dissuaded use of the 8% samples.

Polyvinyl alcohol and PMMA, both types of biocompatible plastic, were added to dissolved 6% w/v chitosan samples to increase sample stability further. PMMA yielded a more useable product, so 2% w/v PMMA was added to the 6% w/v chitosan sample used in further analysis. Lastly, 2% w/v of 2-hydroxyethyl starch was dissolved into the PMMA/chitosan sample to finalize the structural stability.

Fig. 1 demonstrates the chemical synthesis used to formulate the nanocomposite bone sample. The final samples were shaped as described in the *Methods* section and imaged using SEM (Fig. 2). Molecular purity and chemical similarity to bone was confirmed via FTIR (Fig. 1B).

SEM analysis

While the 6% chitosan sample was most durable, it still needed to be compared to the native mammalian bone Fig. 2. As shown, the 6% crosslinked sample had a much more even texture than the noncrosslinked chitosan samples. Even when zoomed to 15,000×, this characteristic description stays accurate, and is similarly textured to the mammalian bone. This texture similarity would translate directly to improved tensile strength and osteoinductive potential [3].

Three-point analysis results

Samples were placed onto the two bottom pressure points while a third shaft applied force to the middle of the sample. The noncrosslinked nanocomposite sample withstood an average of 1.4N of downwards force before beginning to crack, eventually bending to such an extreme that the experiment was manually ended (Fig. 3A). The crosslinked nanocomposite withstood a significantly greater amount of force than the noncrosslinked sample, and compared much more favourably to the actual mammalian bone sample (Fig. 3B and C). The average breaking point occurred when

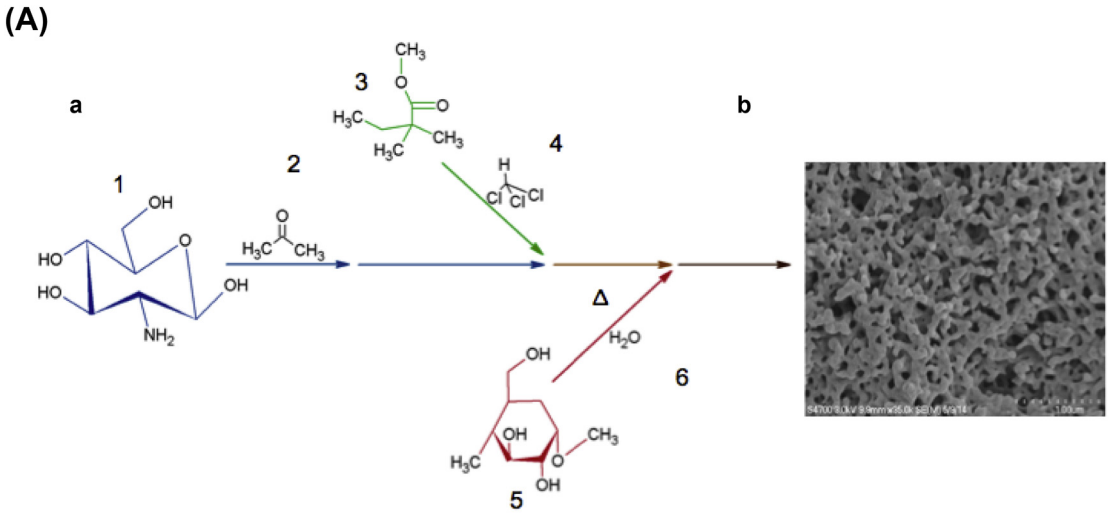

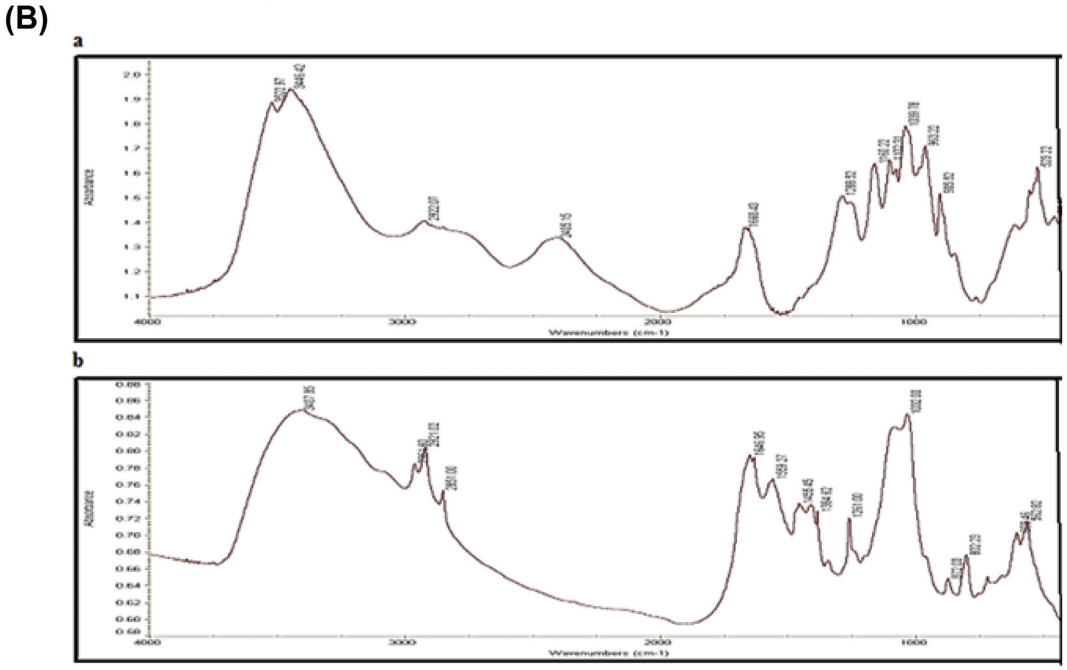

Figure 1 (A) Chemical synthesis of crosslinked nanocomposite material resulting in a morphologically desirable nanocomposite material. (a) A chitosan starting material (blue) was dissolved in acetic acid and combined with a dissolved poly-methylmethacrylate (PMMA; green) mixture in chloroform to form a slurry. 2-Hydroxyethyl starch (red) dissolved in heated water was then combined with the slurry. (b) Magnified 6% chitosan nanocomposite sample. The porous nature of the sample provides ample room for nutrient passage and waste disposal. Scale bar 1 μm; 35,000× magnification. (B) Fourier transformed infrared spectroscopy analysis of the mammalian bone sample and the crosslinked nanocomposite. (a) Nanocomposite sample showing characteristic peaks of the three contributing elements: chitosan, starch, and PMMA. Amine peaks from chitosan can be seen at 3500—3300 cm^{-1}, ester contributions from PMMA can be observed at 1750—1735 cm^{-1}, and alcohol, alkyl, and ether peaks that are present in all samples can be seen at 3550—3200 cm^{-1}, 2950—2850 cm^{-1}, and 1250—1030 cm^{-1}. (b) Mammalian bone sample. Carbonate-to-phosphate ratio areas can be seen at 850—890 cm^{-1}, crystallinity peak areas can be seen at 1000—1100 cm^{-1}, and mineral-to-matrix ratios can be seen at 900—1200 cm^{-1}. (For interpretation of the references to colour in this figure legend, the reader is referred to the web version of this article.)

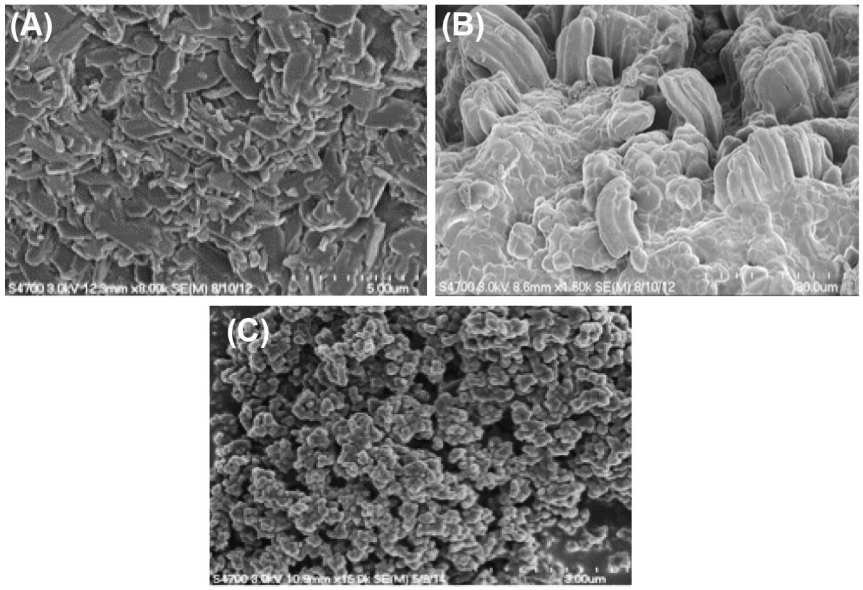

Figure 2 Scanning electron microscope images of the mammal bone and nanocomposite samples. (A) Mammal bone. Scale bar 5 μm; 8000× magnification. (B) 6% chitosan sample, not crosslinked. Note the random indentations and uneven protrusions from the surface, producing a coarse sample. Scale bar 20 μm; 1800× magnification. (C) 6% chitosan sample, crosslinked. The structural surface homogeneity is very similar to the natural mammal bone. Scale bar 3 μm; 15,000× magnification.

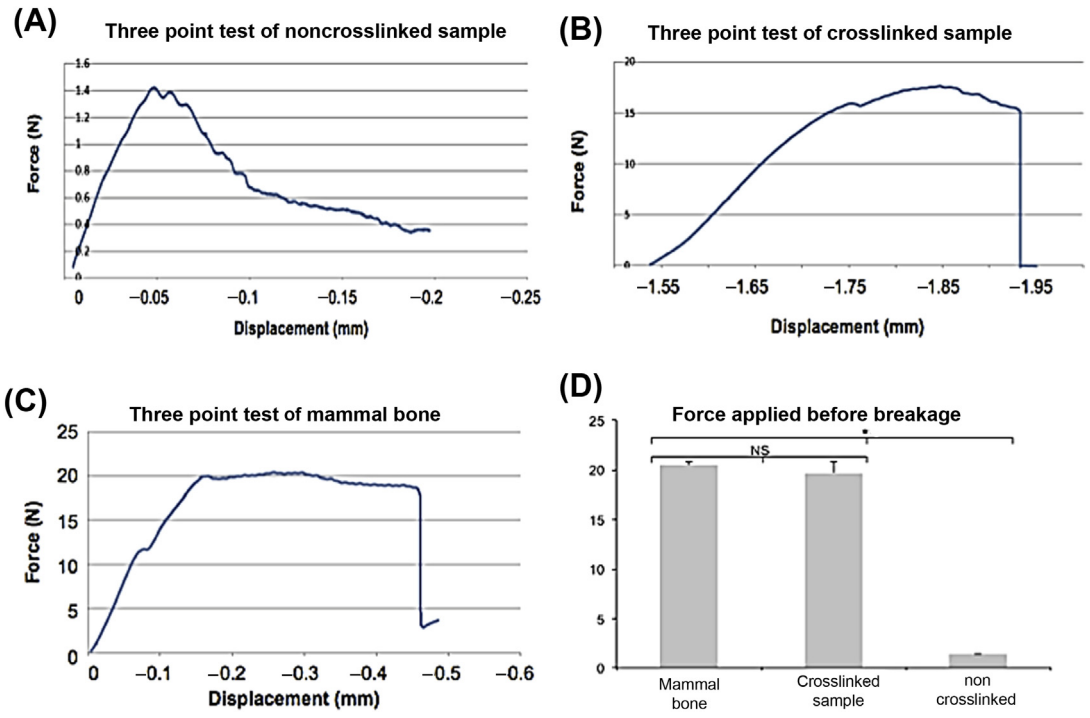

Figure 3 Three-point analysis tests of nanocomposite and murine samples. (A) Representative noncrosslinked nanocomposite sample. The experiment was ended because the sample deformed beyond analysis. (B) Representative crosslinked nanocomposite samples and (C) representative mammalian femur samples withstood a much greater force application before breakage, producing curves indicative of standard force/displacement graphs. (D) Force comparisons across multiple samples. There was no significant difference in average force before breakage between the mammalian femur and the crosslinked sample ($p = 0.228$). Both the mammalian femur and crosslinked samples were significantly stronger than the noncrosslinked nanocomposite sample. $N = 3$. *$p < 0.002$ via analysis of variance and t test. NS = not statistically significant.

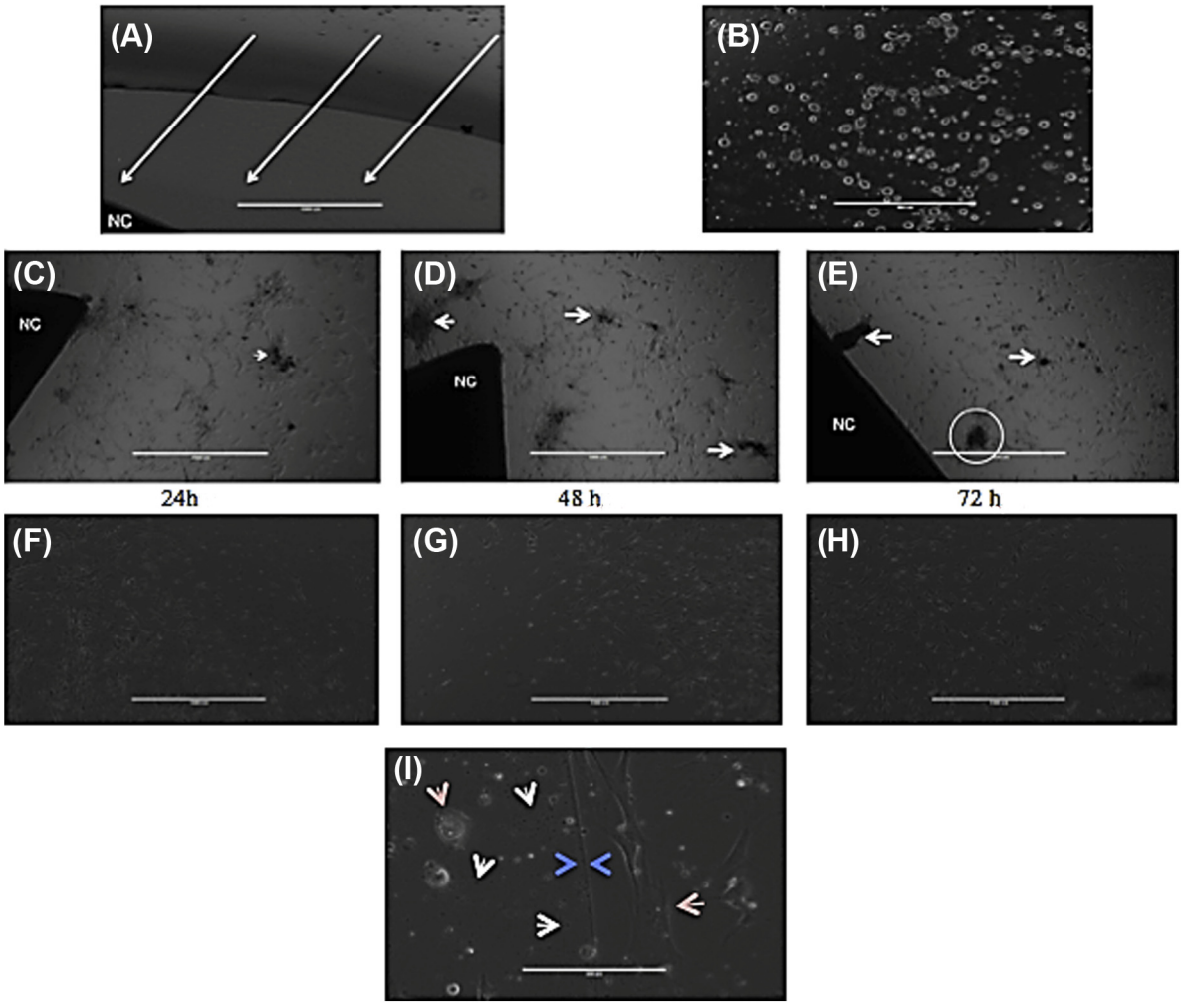

Figure 4 Bone marrow mesenchymal stem cell (BMSC) differentiation over a 72-hour culture period. (A) BMSCs were imaged 2 hours after seeding to show gap zone between nanocomposite material (labeled NC) and seeded BMSCs, approximately 2 mm. Arrows indicate hypothesized direction of stem cell migration. Scale bar 1000 μm; magnification 4×. (B) 10× magnification of the direct culture after 2 hours. All cells have adhered to the culture dish surface but have not begun to proliferate. Scale bar 200 μm. (C—E) Cells 24 hours, 48 hours, and 72 hours, respectively, after seeding. Notice how cells have migrated past the gap zone towards the composite material (labeled NC). Mineralization produced by differentiated cells are indicated by white arrowheads. In (E), the circled area is the focus of Fig. 5. Scale bar 1000 μm; magnification 4×. (F—H) Cells on the fringe of the culture area 24 hours, 48 hours, and 72 hours, respectively, after seeding. Note the lack of mineralization and differentiation of cells. (H) Dark spot on bottom right is due to camera error, not mineralization. Scale bar 1000 μm; magnification 4×. (I) Boundary region observed between cells differentiated due to the bone composite versus those due to culture conditions. Tan arrows indicate cell morphology differences; white arrows point to floating composite material dissolved off of the main block; blue arrows indicate boundary line. Scale bar 200 μm; magnification 10×. (For interpretation of the references to colour in this figure legend, the reader is referred to the web version of this article.)

there was a downwards displacement of 1.84 mm, and a downwards force of 18.6N. The mouse femur control had an average breaking point when there was a downwards displacement of 0.47 mm and a downwards force of 20.07N (Fig. 3C). No statistical difference was observed between the crosslinked sample and the mammalian bone ($p = 0.228$), but both samples were significantly stronger than the noncrosslinked nanocomposite ($p < 0.002$; Fig. 3D).

Biocompatibility

To be an ideal *in vivo* material, an engineered bone composite must be biocompatible. We sought to determine whether the developed composite material was able to be successfully cocultured with BMSCs, proving biocompatibility, and whether the nanocomposite had any influence on BMSC differentiation. BMSCs were seeded approximately 2 mm from the crosslinked composite material (Fig. 4A) and incubated for 72 hours. After 24 hours, perceived mineralization was readily apparent around the composite material (Fig. 4C) compared to cells growing along the fringe elements away from the composite (Fig. 4F). The composite material stimulated cell migration towards itself, prompting increased differentiation and mineralization as the cells came in closer proximity to the nanocomposite (Fig. 4C—E). Neither the composite material nor the culture

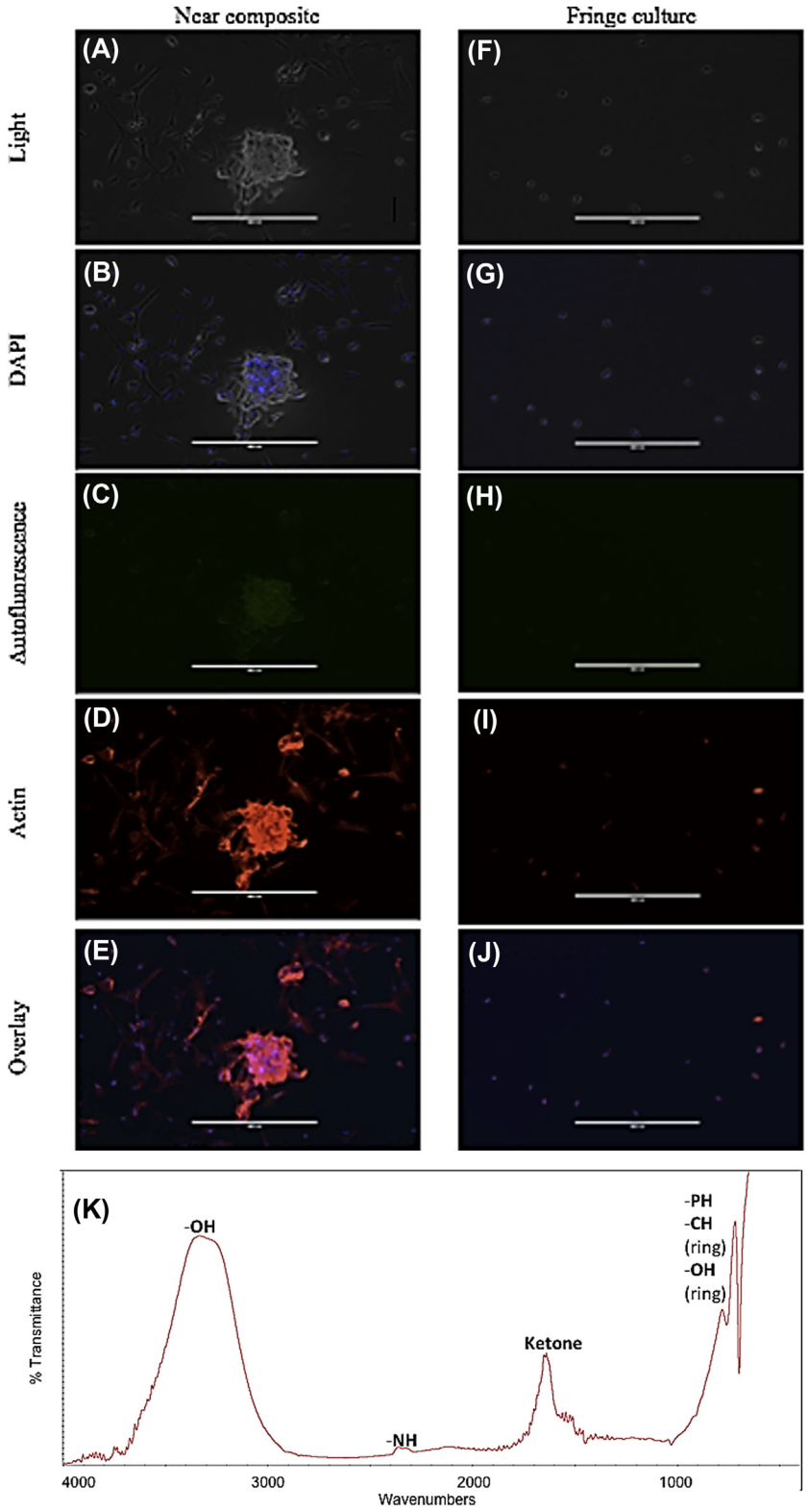

Figure 5 Analysis of culture 72 hours postseed. (A—E) Cells and mineralization from an area adjacent to bone composite (see circled portion in Fig. 4E). (F—J) Cells on the fringe of the culture dish with little to no contact with bone composite material. (A, F) Light microscope; (B, G) DAPI filter of NucBlue stain; (C, H) 470 nm/525 nm filter of autofluorescence of bone composite material surrounding cells and embedded in the mineralised component; (D, I) 531nm/593nm filter of ActinRed 555 stain; (E, J) overlay of autofluorescence and stains. (K) Fourier transformed infrared spectra of one bone nodule produced by bone marrow-derived mesenchymal stem cell culture. Peaks indicative of phosphate-to-carbonate ratio area and cortical bone similarities are highlighted. (For interpretation of the references to colour in this figure legend, the reader is referred to the web version of this article.)

conditions were detrimental to cell growth, as proliferation was seen around the composite (Fig. 4C—E) and in the untreated portions of the dish (Fig. 4F—H). Interestingly, a differentiation boundary was observed after 48 hours (Fig. 4I). As deemed by DAPI filters and autofluorescence, this boundary was formed from dissolved composite material and spread out in a halo around the composite (data not shown). The conditions within and beyond this boundary were profoundly different, changing cell morphology and culture viscosity (Fig. 4I, arrows).

After 72 hours, the media was removed and the cells were fixed and stained as described in the *Methods* section. Two contrasting culture areas were imaged (Fig. 5): an area of high cell growth and biomaterial deposition (highlighted in Fig. 4E; analysed in Fig. 5A—E) was compared to a fringe portion of the culture several centimetres from the composite bone (Fig. 5F—J). The mineralization area showed increased cell density and differentiation (Fig. 5A and B), with increased F-actin production indicative of immature osteogenic differentiation to osteoblasts (Fig. 5D) [20]. By contrast, cells on the periphery of the culture on the opposite side of the differentiation boundary, showed limited cellular hypertrophy and proliferation (Fig. 5F and G), and only the requisite amount of β-actin to maintain cellular morphology (Fig. 5I). The high cell growth and deposition area also showed an autofluorescence when observed under the 470 nm excitation/525 nm emission filter of the Evos FL (Fig. 5C), and the fringe area showed little to no autofluorescence (Fig. 5H). When examined under FTIR, the deposition material produced a spectra almost identical to young cortical bone (Fig. 5K; Rhonda Prisby and Arun Kumar, unpublished data), potentially indicating the beginnings of bone formation *in vitro*.

Discussion

The role of nanomedicine in biomedical and tissue engineering applications is becoming increasingly apparent with the advent of more biocompatible structures that aid in cell growth and stem cell differentiation. However, issues may arise when developing structures that will implant to a system with disproportionately large loading forces, such as the femur bone.

Analysis of the SEM images brought results suggesting that the crosslinked 6% chitosan sample more closely resembles the texture of the mammal bone. This is pertinent to the final goal because, as previously shown [21], texture plays a key role in osteoblast adherence and proliferation to bone composites. The more porous nature of the nanocomposite (Fig. 2B) will allow nutrient and waste exchange with the outside environment, allowing full thickness seeding of the composite material. This will assist in quicker cell growth and promote the native bone to overtake the nanocomposite. The porous nature will also require little biodegradation before vasculature can permeate the sample, which is crucial, as angiogenesis is the key to promoting efficient bone growth [22].

Perhaps the most important aspect of any graft of composite bone material is its ability to withstand the forces applied by the human body during day-to-day activities. While pressure on bones significantly varies depending on the level and type of activity [23], the femur is an ideal model as it is both the strongest and longest bone in any mammalian system [24,25]. Therefore, any composite material that can withstand three-point analysis testing comparative to a femur sample would theoretically be able to be scaled back *in vitro* in order to realistically match and support more pliable bones. Indeed, our crosslinked sample was more flexible than our mammal bone control (as seen by the extent of shaft displacement), a desirable characteristic that will allow more flexibility *in vivo*. The flexibility would be worrisome if it came at the expense of strength, but the analysis showed no difference in the crosslinked sample compared to the mammalian bone. As is, the crosslinked nanocomposite sample is comparable to other studies using femurs and ulnas [26]. Since bone mineral density and strength decrease with age [27], the composite material could theoretically be successfully used in repair of fractures in the elderly. The Young's modulus of the crosslinked sample was also not significantly different from the mammalian bone (data not shown). While the current nanocomposite and mammalian femur demonstrated Young's moduli of the order of tenths of a GPa, scaling up the material to the size of a human cortical or trabecular bone would presumably allow for Young's modulus values to reach the requisite 14—20 GPa needed for full support [28].

The boundary area during cell culture was a surprising development in the analysis. While it was hypothesized that the cells would migrate towards the biocompatible bone composite and begin to differentiate, the effects of the nanocomposite were expected to dissipate in a concentration dependent manner, not at an abrupt line. This is a beneficial addition to future data, as the size of this boundary region could be controlled to develop a microenvironment around the nanocomposite *in vivo* that would control the extent of osteoinduction and eliminate any system-wide effects. Our results show that there is potential for osteoinduction based on F-actin staining [20], but further molecular analysis is needed before claims of osteoinduction of BMSCs can be verified. The autofluorescence of the nanocomposite material was observed prior to staining (data not shown), and was used as a marker to show interactions between the cell material and the dissolved nanocomposite (Fig. 5C). Also surprising was the autofluorescence under the 470 nm/525 nm filter after washing and fixing. We hypothesise that the nanocomposite dissolved into solution (as shown by the boundary region) and bound to the cells through a receptor, such as the $\alpha 1\beta 1$ integrin, that has been previously shown to steer stem cells down the osteogenic pathway [29]. The attachment of the nanocomposite material to the BMSCs/osteoblasts shows a very high dissociation constant and avidity of the material to the receptors, as indicated by time-in-culture analysis and adherence following fixation and staining. The elucidation of the respective receptors on the BMSCs (and ultimately

osteoblasts) could lead to a new drug target to promote osteogensis in osteoporotic individuals.

Conclusion

The goal of this study was to develop a nanocomposite material that compared favourably to an actual mammalian bone sample. We successfully developed two samples: a noncrosslinked and a crosslinked 6% chitosan/2% PMMA/2% starch sample. The crosslinked sample was superior to the noncrosslinked sample in strength, chemical, and microscopic analysis. When deposited next to cultures of BMSCs, the nanocomposite material showed biocompatible tendencies by promoting migration and proliferation of BMSCs. Mineralized nodule deposits into culture by the differentiated BMSCs showed spectroscopically similar results to extracted mammalian cortical bone, indicating new bone formation. Future genetic and molecular analysis, such as alkaline phosphatase activity and polymerase chain reaction, will determine whether cellular deposition is indicative of osteogenic differentiation, proving that the nanocomposite is also osteoinductive.

Conflicts of interest

The authors declare no competing financial interests.

Funding/support

Dr. Kumar would like to acknowledge the startup funding and UDRF (University of Delaware Research Foundation) Award he received from the University of Delaware.

References

[1] Messora MR, Nagata MJ, Pola NM, de Campos N, Fucini SE, Furlaneto FA. Effect of platelet-rich plasma on bone healing of fresh frozen bones allograft in mandibular defects: a histomorphometric study in dogs. Clin Oral Implants Res 2012;24:1347—53.
[2] Colvin RB, Smith RN. Antibody-mediated organ-allograft rejection. Nature Rev Immunol 2005;5:807—17.
[3] Lo KWH, Ulery BD, Ashe KM, Laurencin CT. Studies of bone morphogenetic protein based surgical repair. Adv Drug Deliv Rev 2012;64:1277—91.
[4] Evans CH. Gene delivery to bone. Adv Drug Deliv Rev 2012;64:1331—40.
[5] Demers C, Hamdy CR, Corsi K, Chellat F, Tabrizian M, Yahia L. Natural coral exoskeleton as a bone graft substitute: a review. Biomed Mater Eng 2002;12:15—35.
[6] Lee MJ, Sohn SK, Kim KT, Kim CH, Ahn HB, Rho MS, et al. Effect of hydroxyapatite on bone integration in a rabbit tibial defect model. Clin Orthop Surg 2010;2:90—7.
[7] Spalazzi JP, Doty SB, Moffat KL, Levine WN, Lu HH. Development of controlled matrix heterogeneity on a triphasic scaffold for orthopedic interface tissue engineering. Tissue Eng 2006;12:3497—508.
[8] Moore WR, Graves SE, Bain GI. Synthetic bone graft substitutes. ANZ J Surg 2001;71:354—61.
[9] Albrektsson T, Johansson C. Osteoinduction, osteoconduction and osseointegration. Eur Spine J 2001;10:S96—101.
[10] Jaiswal N, Haynesworth SE, Caplan AI, Bruder SP. Osteogenic differentiation of purified, culture-expanded human mesenchymal stem cells *in vitro*. J Cell Biochem 1997;64:295—312.
[11] Morgado J, Pereira AT, Bragança AM, Ferreira Q, Fernandes SCM, Freire CSR, et al. Self-standing chitosan films as dielectrics in organic thin-film transistors. Express Polym Lett 2013;7:960—5.
[12] Hu Q, Li B, Wang M, Shen J. Preparation and characterization of biodegradable chitosan/hydroxyapatite nanocomposite rods via *in situ* hybridization: a potential material as internal fixation of bone fracture. Biomaterials 2004;25:779—85.
[13] Struszczyk H, Wawro D, Niekraszewicz A. Advances in chitin and chitosan. London: Elsevier Applied Science; 1991.
[14] Illum L. Chitosan and its use as a pharmaceutical excipient. Pharm Res 1998;15:1326—31.
[15] Dai T, Tanaka M, Huang YY, Hamblin MR. Chitosan preparations for wounds and burns: antimicrobial and wound-healing effects. Expert Rev Anti Infect Ther 2011;9:857—79.
[16] Lee JW, Kim SY, Kim SS, Lee YM, Lee KH, Lee SJ. Synthesis and characteristics of interpenetrating polymer network hydrogel composed of chitosan and poly(acrylic acid). J Appl Polym Sci 1999;73:113—20.
[17] Su N, Chen M, Chen S, Li C, Xie Y, Zhu Y, et al. Overexpression of H1 calponin in osteoblast lineage cells leads to a decrease in bone mass by disrupting osteoblast function and promoting osteoclast formation. J Bone Miner Res 2013;28:660—71.
[18] Wang TJ, Wang IJ, Lu JN, Young TH. Novel chitosan-polycaprolactone blends as potential scaffold and carrier for corneal endothelial transplantation. Mol Vis 2012;18:255—64.
[19] Bhat S, Tripathi A, Kumar A. Supermacroprous chitosan—agarose—gelatin cryogels: *in vitro* characterization and *in vivo* assessment for cartilage tissue engineering. J R Soc Interface 2011;8:540—54.
[20] Ashori A, Cordeiro N, Faria M, Hamzeh Y. Effect of chitosan and cationic starch on the surface chemistry properties of bagasse paper. Int J Biol Macromol 2013;58:343—8.
[21] Tsao CW, Hromada L, Liu J, Kumar P, DeVoe DL. Low temperature bonding of PMMA and COC microfluidic substrates using UV/ozone surface treatment. Lab Chip 2007;7:499—505.
[22] Flores-Ramírez N, Luna-Bárcenas G, Vásquez-García SR, Muñoz-Saldaña J, Elizalde-Peña EA, Gupta RB, et al. Hybrid natural-synthetic chitosan resin: thermal and mechanical behavior. J Biomat Sci Polym Ed 2008;19:259—73.
[23] Costa-Pinto AR, Reis RL, Neves NM. Scaffolds based bone tissue engineering: the role of chitosan. Tissue Eng Part B Rev 2011;17:331—47.
[24] Towler DA. The osteogenic-angiogenic interface: novel insights into the biology of bone formation and fracture repair. Curr Osteoporos Rep 2008;6:67—71.
[25] Kohrt WM, Barry DW, Schwartz RS. Muscle forces or gravity: what predominates mechanical loading on bone? Med Sci Sports Exerc 2009;41:2050—5.
[26] Cummings SR, Black DM, Nevitt MC, Browner W, Cauley J, Ensrud K, et al. Bone density at various sites for prediction of hip fractures. The Study of Osteoporotic Fractures Research Group. Lancet 1993;341:72—5.
[27] Silva MJ, Brodt MD, Lynch MA, McKenzie JA, Tanouye KM, Nyman JS, et al. Type 1 diabetes in young rats leads to progressive trabecular bone loss, cessation of cortical bone growth, and diminished whole bone strength and fatigue life. J Bone Miner Res 2009;24:1618—27.
[28] Boskey AL, Coleman R. Aging and bone. J Dent Res 2010;89:1333—48.
[29] Rosa AL, Kato RB, Castro Raucci LM, Teixeira LN, de Oliveira FS, Bellesini LS, et al. Nanotopography drives stem cell fate toward osteoblast differentiation through $\alpha 1\beta 1$ integrin signaling pathway. J Cell Biochem 2014;115:540—8.